COMBUSTION SCIENCE AND TECHNOLOGY
2021, AHEAD-OF-PRINT, 1-17
https://doi.org/10.1080/00102202.2021.2013830

Soot Formation and Growth in Toluene/Ethylene Combustion Catalyzed by Ruthenium Acetylacetonate

Fanggang Zhang [a], Cong Wang [a], Juan Wang [a], Sönke Seifert [b], and Randall E. Winans [b]

[a] School of Energy and Power Engineering, Beihang University, Beijing. PR China [b] X-ray Science Division, Advanced Photon Source, Argonne National Laboratory, Argonne, Illinois, USA

ABSTRACT

Ruthenium-based compounds are efficient catalysts to enhance combustion performance and suppress soot emission. However, systematic mechanism and *in-situ* research on reducing soot are rarely addressed. In this study, ruthenium acetylacetonate ($Ru(C_5H_7O_2)_3$, $Ru(acac)_3$) was utilized as the catalyst precursor in different concentration conditions to investigate its impacts on the size, volume, and morphology of the soot particles in the ethylene flames with central toluene injection. The soot particles were detected by *in-situ* small-angle X-ray scattering (SAXS) and *ex-situ* transmission electron microscopy (TEM). This study confirms that $Ru(acac)_3$ can suppress the surface growth for the primary soot particles, but no significant change of the morphology has been discovered for the aggregates. Compared with the undoped flame, the volume of the soot particles in the $Ru(acac)_3$-doped flames is lower and the particle size is smaller, indicating a valid inhibition effect of $Ru(acac)_3$ on the soot emission by affecting its surface growth and oxidation process. Despite the remarkable distinction between the undoped and doped flames, no obvious difference is found between the flames with different catalyst concentrations.

ARTICLE HISTORY
Received 22 September 2021
Revised 29 November 2021
Accepted 30 November 2021

KEYWORDS
Soot, catalyst, ruthenium acetylacetonate, surface growth, oxidation, *in-situ* small angle X-ray scattering

CONTACT Juan Wang juanwang@buaa.edu.cn School of Energy and Power Engineering, Beihang University,Beijing 100191, PR China

Introduction

Soot particles, of particular concern in the environment pollution, impact human health negatively. Inhalation of soot particles might cause respiratory diseases, cardiovascular diseases, pulmonary function loss, or even death (Guaita et al. 2011). They also have a serious effect on environment and global warming (Tollefson 2013). In addition, carbon deposition on the engine's inner wall, fuel nozzle, and other places caused by incomplete combustion reduces combustion efficiency and engine performance. Therefore, there is an urgent need to solve soot emission issue efficiently.

Enhancing soot oxidation is an efficient way to suppress emission of soot particles. Metal-based catalysts exhibit a vital potentiality in soot elimination and have been widely used in catalytic soot combustion over the past years. Many investigations have demonstrated that noble metals and their modified catalysts (Lee et al. 2018; Oi-Uchisawa et al. 2000; Ren et al. 2019), alkaline metal (Li et al. 2012, 2016), transition metals (Howard and Kausch 1980; Hu et al. 2017) and metal oxides (Gao et al. 2018; Neeft, Makkee, Moulijn 1996) are capable to enhance soot oxidation. Marsh et al. (2007)indicated that ferrocene, ruthenocene, iron naphthenate, and methylcyclopentadienyl manganese tricarbonyl (MMT) are quite effective in soot

reduction in JP-8 lean flames. Likewise, Kim and Hahn (2016) reported that the catalytic effect of iron compounds can greatly reduce activation energy for soot oxidation reaction. In addition, Wei and Lee (1999) conducted a pyrolysis experiment of polystyrene doped with $MnSO_4$ in inert conditions, and they pointed out that $MnSO_4$ addition decreased the amount of Polycyclic Aromatic Hydrocarbons (PAHs) due to the transition metal chelation oxidation mechanism. In our recent study (Tang et al. 2019), an *in-situ* study was performed regarding effects of nickel acetylacetonate on soot inception and growth in an ethylene flame with toluene injection. It was found that Ni additive reduced the primary soot particle size and soot volume fraction significantly, and the additive also delayed the soot surface growth, eventually leading to the primary soot particles with rough surfaces. To explore catalysts for reducing soot emission more efficiently, investigations on a series of catalysts and further studies of detailed catalytic mechanism are needed.

Platinum group metals behave as effective catalysts in soot reduction (Castoldi et al. 2017; Yashnik and Ismagilov 2019). Ruthenium is the cheapest metal in the platinum group and it has been used in soot control. Castoldi et al. (2017) found that the ruthenium catalyst promotes soot oxidation by roughly 90% and the Ru-based catalyst has higher activity in the soot combustion than the Pt-based catalyst. Besides, there are also many studies demonstrating that the catalytic reactivity of the metal oxide catalysts for soot oxidation was significantly enhanced by doping with Ru nanoparticles (Aouad et al. 2007; Ledwa, Pawlyta, Kepinski 2018; Nascimento et al. 2014). The temperature of carbon-black oxidation decreased by 100–150°C after the addition of ruthenium to ceria as the catalyst (Aouad et al. 2007). However, all of these experimental studies related to the impacts of Ru-based catalysts on soot particles are *ex-situ*. To understand the mechanism how Ru-based catalysts impact the soot particles and further improve the design of catalysts, it is essential to perform experiments by *in-situ* measurement.

In this work, $Ru(acac)_3$ of different concentrations was used as the organometallic catalyst precursor in ethylene base flames with central toluene injection. $Ru(acac)_3$ was selected as the Ru-based catalyst precursor because it is soluble in toluene. Synchrotron small-angle X-ray scattering (SAXS) was used to *in-situ* detect the information of the size, morphology, and volume fraction of the soot particles, and the data were analyzed by fitting the scattering intensities based on SAXS theory. Till now, many researchers have shown interest in investigating soot and fuel-soluble metal catalysts by utilizing SAXS (Braun et al. 2004; Di Stasio 2017; Mitchell et al. 2009; Tang et al. 2019; Wang et al. 2015; Yon et al. 2018). It is worth mentioning that this is the first study to *in-situ* investigate the effects of Ru-based catalysts on the soot particles. As a complementary method, transmission electron microscopy (TEM) was used to study the morphological and structural properties of soot, and the particle statistical size distribution.

Experimental Methods

Experimental setup

In this study, the SAXS experiments were conducted on the beamline 12-ID-C at the Advanced Photon Source in Argonne National Laboratory, USA. An 8 keV incident X-ray with 0.6 mm in width and 0.1 mm in height was used. The experimental exposure time was 0.5 s and the SAXS signals were recorded by the CCD detector with a resolution of 2048 × 2048 pixels and normalized by the incident photon intensity. The 2D platinum CCD detector was 2 m away from the flame. The transmitted X-ray beams were blocked by a beam stop before they arrived at the detector.

A Hencken burner was used in our experiments as shown in Figure 1. As can be seen in the enlarged figure of the burner surface, the diameter of each fuel tube is approximately 0.5 mm, while the oxygen tubes are regular hexagonal in cross-section with 0.4 mm each side length. The total cross-section area of the fuel and oxygen flow is 25.4 × 25.4 mm, shielded by a 6.3 mm wide nitrogen co-flow at 7.730 L/min. The flow rates of ethylene and oxygen were 0.159 and 0.400 L/min, respectively. Another nitrogen line at 0.900 L/min was mixed with oxygen before flowing into the burner. Different concentrations of $Ru(acac)_3$

were dissolved in toluene (50, 100, 150 ppm by weight) and the solution was aerosolized by an aerosol generator (SONAER, Inc., 241PG). The solution was aerosolized at a rate of 0.063 mL/min, and then carried into a 1 mm inner diameter central tube of the burner by nitrogen at 0.114 L/min. It should be noted that a Hencken burner is to generate flat flames over the fuel injection region in normal operation. However, in this study, the flame is more like a laminar jet flame with the toluene solution injected from the central tube. And toluene was used in all cases to enable the fuels' concentrations are the same for both doped and undoped flames.

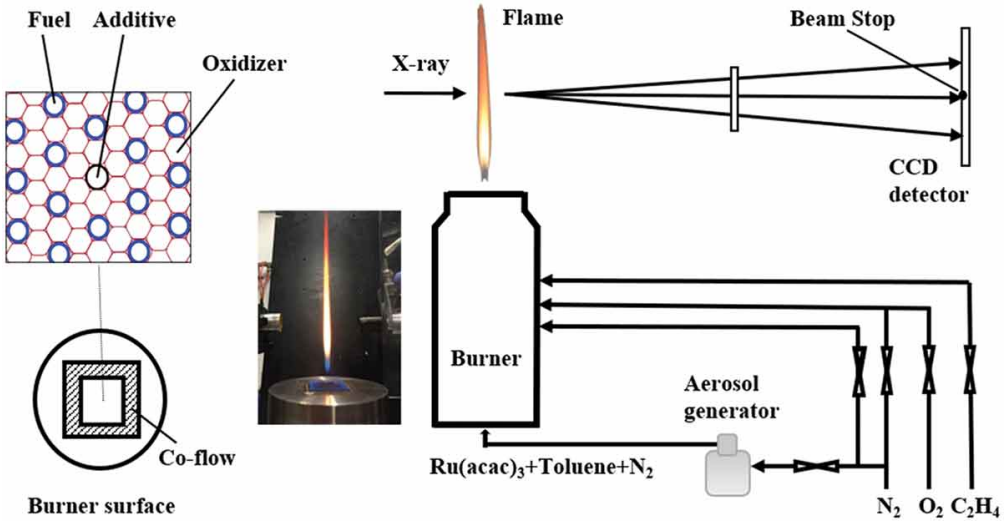

Figure 1. Schematic layout for the SAXS experiments

Data analysis of SAXS

SAXS is an online noninvasive detection approach that is particularly useful in studying the size distribution and structure of soot particles. The scattered intensity $I(q)$ mainly relies on the size, shape, and number density N of particles in a dilute suspension where the internal reactions can be neglected. The basic equation for $I(q)$ versus the scattering vector q is given by

$$I(q)= N[F(q)]^2 \tag{1}$$

where $F(q)$ is the coherent sum of the scattering amplitudes of the individual scattering centers within the particle given by the Fourier transform of the electron density distribution (Brumberger 2013). The scattering vector q is defined as

$$q =(4\pi/\lambda)\sin(\theta/2) \tag{2}$$

where λ is the wavelength of the incident X-ray and θ is the scattering angle.

For values of $qR_G< 1$, Guinier et al. (1955) showed

$$I(q)= G\exp\left(-q^2 R_G^2/3\right) \tag{3}$$

where G is the pre-exponential factor given by $\mathbf{G = NV^2 r_e^2 \Delta\rho^2}$, V is the volume of the particle, r_e is the Thomson scattering length equal to the classical electron radius (2.818×10^{-15} m), and R_G is the radius of gyration of a particle relative to its center of gravity. The quantity $\mathbf{\Delta\rho = \rho - \rho_M}$ is the contrast electron density or relative scattering length density of the particles with respect to the medium. A $\ln I\,(\mathbf{q})$ vs q^2 plot, i.e., the Guinier plot, can be obtained by taking the logarithm of Eq. (3), which is well-known used in small-angle scattering for determining R_G.

Another expression of $I(q)$ is proposed when $qR_G \gg 1$,

$$I(q) = 2\pi r_e^2 N \Delta\rho^2 S q^{-4} \tag{4}$$

where S is the particle surface area. Eq. (4) refers to the Porod region, and the Porod exponent P that related to the fractal dimension is summarized as follows (Brumberger 2013):

$$I(q) \propto q^{-p} \begin{cases} P = 4 \text{sharpinterface} \\ 3 \le P < 4 \text{surfacefractal} \\ P < 3 \text{massfractal} \\ P \approx 2 \text{gaussianpolymerchain} \end{cases} \tag{5}$$

Beaucage and Schaefer (1994) combined a Guinier and an associated Porod region into a unified exponential scattering function as one level, which can be more generally applied to mass fractal and surface fractal as well as those having smooth surfaces. This function is defined as

$$I(q) = G\exp\left(-q^2 R_G^2/3\right) + B\left\{\left[\text{erf}\left(qR_G/\sqrt{6}\right)\right]^3/q\right\}^p \tag{6}$$

where G is the Guinier pre-exponential factor as indicated above, $\mathrm{B} = 2\pi \mathrm{N} \Delta\rho^2 \mathrm{S}$ is the Porod pre-factor, erf is the error function, and P is the power law slope, i.e., the Porod exponent.

For two-level structures consisting of primary particles (level one) and aggregates (level two), the above equation may be extended to (Beaucage 1995; Beaucage and Schaefer 1994):

$$\begin{aligned} I(q) = {} & G\exp\left(-q^2 R_G^2/3\right) + B\exp\left(-q^2 R_{sub}^2/3\right)\left\{\left[\text{erf}\left(qR_G/\sqrt{6}\right)\right]^3/q\right\}^p \\ & + \mathrm{G_s}\exp\left(-q^2 R_s^2/3\right) + B_s\left\{\left[\text{erf}\left(qR_s/\sqrt{6}\right)\right]^3/q\right\}^{P_s} \end{aligned} \tag{7}$$

where R_s is the radius of gyration for small-scale particles, and these particles agglomerate to form large-scale particles with R_G. Mostly, the value of R_{sub} (the high-q cutoff for the power law region) is identical to R_s. Besides, G_s,B_s and P_s are the corresponding factors for the small-scale particles.

Moreover, the Porod invariant Q is obtained through the integral of the $q^2 \cdot I(q)$ vs q plot (Pilz, Glatter, Kratky 1982),

$$Q = \int_0^\infty I(q) q^2 dq \tag{8}$$

For homogeneous particles, Q is proportional to the volume fraction φ_V of the particles:

$$Q = 2\pi^2 \Delta\rho^2 \varphi_V \tag{9}$$

where $\Delta\rho$ is the difference of the scattering length densities between the medium air and soot. Because the scattering length density of air is much smaller than that of carbon, thus we took $\Delta\rho \approx \rho_{\text{soot}} = 15.26 \times 10^{10}$ cm^{-2} in this study.

The scattering intensity profiles were fitted and analyzed by using Irena tool suite (Ilavsky and Jemian 2009) in Igor Pro software package. Unified fitting method developed by Beaucage and Schaefer (1994) are suitable for polydisperse particles with multiple structure levels and was used to obtain R_G and the Porod exponent P in this work. Besides, the particle volume distribution can be yielded by taking the inverse

Fourier transform of the measured $I(q)$ vs q relation in the total non-negative least-squares (TNNLS) method (Merritt and Zhang 2005). This unified fitting procedure applies an interior-point gradient method to solve the so-called totally nonnegative least-squares problems. Before fitting, the SAXS intensities was needed to be calibrated by subtracting the background, which contains noises scattered from air and instrument windows. It is challenging to subtract a suitable background to get an accurate signal. The gas density in the flame regime is lower than that in the surrounding air, which often lead to an overestimation of the background (Mitchell et al. 2009). In an attempt to compensate for this error, we corrected the scattering curve of the ambient air by reducing the air density at the temperature comparable to the flame, and used this corrected curve as the air background in the flame. Besides, the measured raw intensity data was normalized by the incident photon intensity, sample transmission, and the solid angle subtended by the detector pixels. The scattering intensity of glassy carbon was measured as the standard sample to calibrate the SAXS intensities of the target samples. Thus, we could obtain the absolute scattering intensities of SAXS signals.

Following SAXS analysis of the soot particles, TEM was adopted as a complementary characterization method to identify soot morphology and size. In this work, we collected the soot particles by using C/Cu TEM grids. TEM images (25,000×) were obtained by a 200 kV JEM-2200FS TEM with a Gatan digital camera in University of Science and Technology Beijing. To determine the size distribution and the mean diameter of the primary particles, three hundred particles at least were counted. The primary particles are merged together, so only the particles with strong contrast and clear boundary were picked to determine the particle size.

Results and discussion

Effect of catalysts on soot morphology

TEM images were obtained for the soot particles collected at 30 and 40 mm heights above the burner (HAB) for each flame. The comparisons of the soot morphology between the undoped flame and $Ru(acac)_3$-doped flames are shown in Figure 2. It is observed that the aggregated particles are composed of near-spherical primary particles and behave as long chains with quite loose structure. The particles in the undoped flame are generally larger than those in the 50, 100, and 150 ppm $Ru(acac)_3$-doped flames.

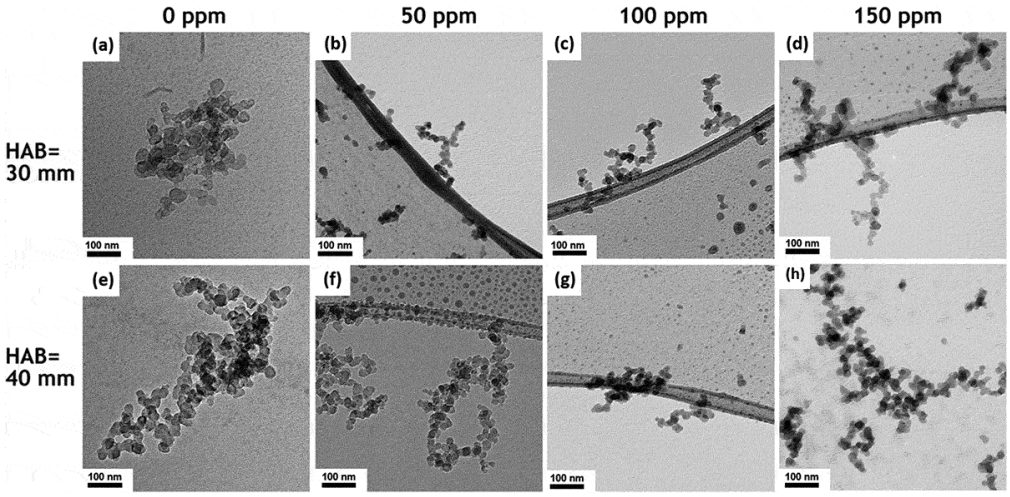

Figure 2. TEM images (25,000× magnification) of the soot particles sampled at HAB = 30 mm, 40 mm of the undoped flame and $Ru(acac)_3$-doped flames. The first row is the soot sampled from 30 mm HAB, and the second row is the soot sampled from 40 mm HAB. (a, e) Undoped flame. (b, f) 50 ppm $Ru(acac)_3$-doped flame. (c, g) 100 ppm $Ru(acac)_3$-doped flame. (d, h) 150 ppm $Ru(acac)_3$-doped flame

In our previous study (Tang et al. 2019), lean flame experiments containing only catalyst particles were conducted, and sooting flames containing both soot and metal particles were also performed. All results showed that the concentration of the metal or metal oxide nanoparticles is very small and below the detection limit of SAXS measurement even in the condition with 450 ppm additive, which is larger than the highest concentration (150 ppm) we chose in this work. Therefore, the SAXS signals in these measurements are only from the soot particles.

The scattering intensities $I(q)$ versus scattering vector q were obtained at q range from about 0.04 to 0.8 nm^{-1}. Considering the correlation $R \sim \pi/q$ (nm), this q range approximately corresponds to particle radius from 4 to 79 nm including primary particles and small aggregates. Figure 3 presents the selected scattering curves at 20, 25, 30, 35 and 40 mm HAB, respectively. It is noted that the scattered intensities are close to each other at HAB above 40 mm, which makes it difficult to compare individual scattering curves at different HABs. Thus, only the scattered intensities below 40 mm are presented. It is obvious that $I(q)$ increases with increasing HAB for each flame, indicating the total volume of the soot particles increases with increasing HAB. Detailed discussions after data fitting using SAXS theory are presented later. Comparing the undoped flame with the doped flames in different concentration conditions, it can be seen that $I(q)$ decreases significantly with $Ru(acac)_3$ dopant. The intensity uncertainties including the measured systematic errors and errors from the data reduction are shown in Figure 3(b). It can be seen that the uncertainties are much smaller than the differences between any two profiles. So the uncertainties do not affect the trends of the curves at different HABs. Since the uncertainties are so small, we do not show them in other figures.

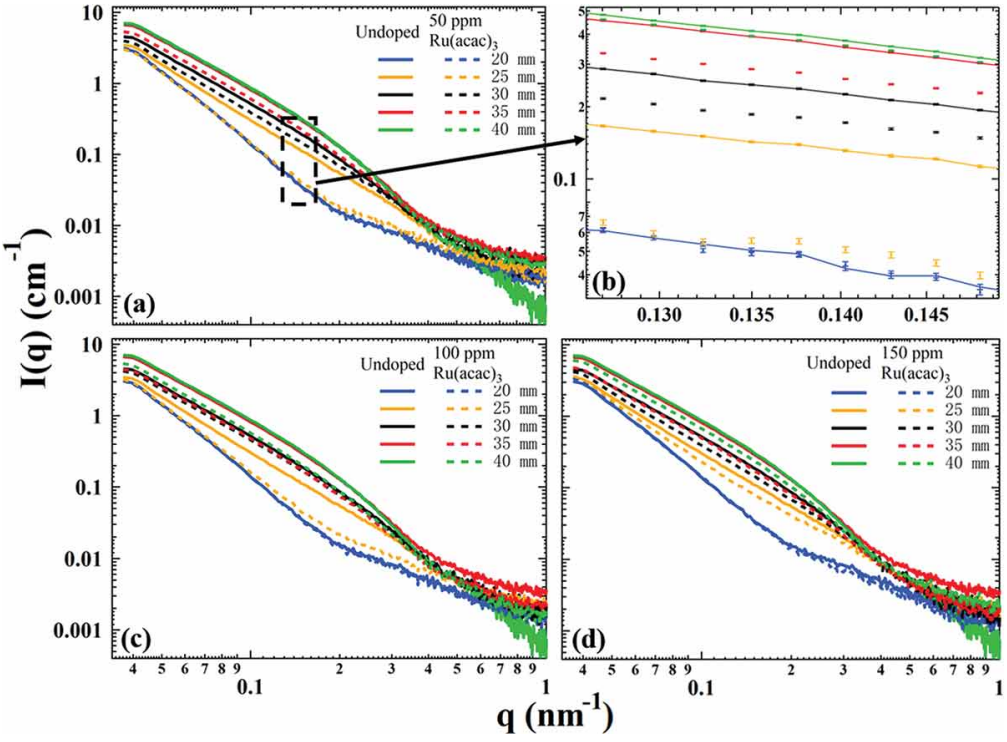

Figure 3. $I(q)$ of the soot particles in the undoped and doped flames at 20, 25, 30, 35 and 40 mm HAB, respectively. (a) Comparison between the undoped and 50 ppm $Ru(acac)_3$-doped flames. (b) Enlarged figure of Figure 3(a) with uncertainties. (c) Comparison between the undoped and 100 ppm $Ru(acac)_3$-doped flames. (d) Comparison between the undoped and 150 ppm $Ru(acac)_3$-doped flames

It seems that the scattering intensities below 27 mm HAB are approximate to the background curve, which makes it difficult to fit. Thus, only the fitting results of the scattering curves in the range of 27—40 mm are presented. Figure 4 presents such an example of the application of unified fitting at HAB = 35 mm. Each term appearing in Eq. (7) is represented by different colored lines in the figure. Due to the limit of the

SAXS measurement range, only the primary particles for level 1 at high q and the power law region of the soot aggregates for level 2 at low q can be detected in our measurement. The Guinier region of level 2 is omitted by setting G to 0 and R_G is automatically set to 10^{10}. Therefore, we can obtain the size and morphology information of the primary particles for level 1, and some morphology information of the aggregates for level 2 can also be acquired in this study. Unfortunately, large aggregates are out of the measurement range in this work

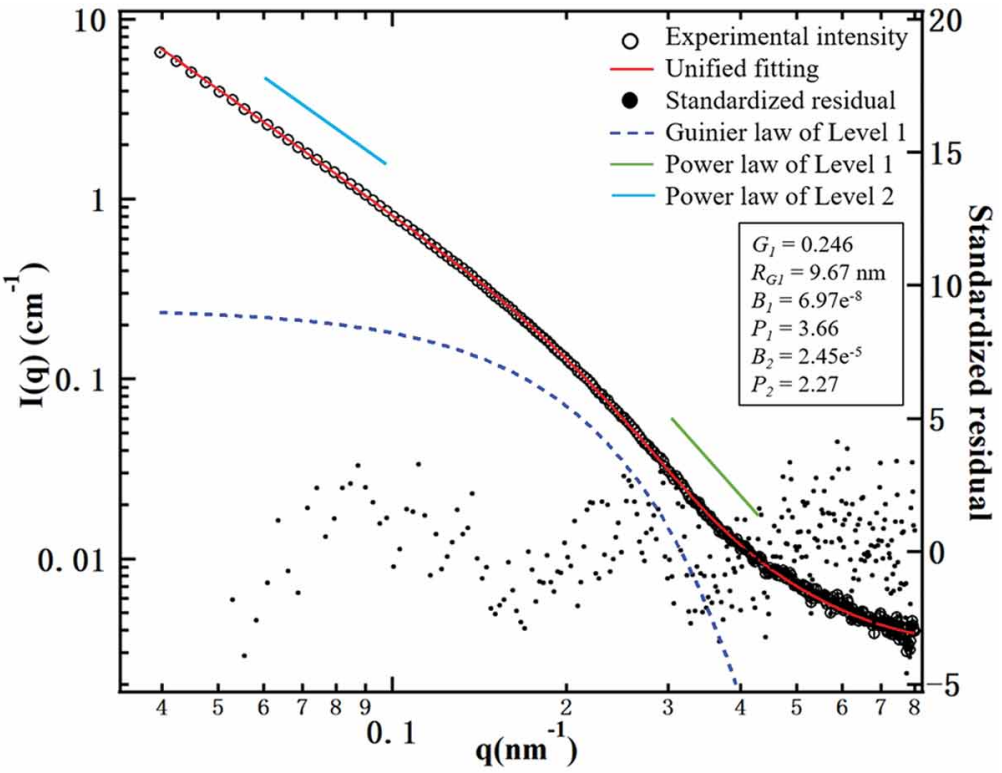

Figure 4. An example of unified fitting of SAXS scattering intensity at HAB = 35 mm

.

The Porod exponent P was obtained from the two-level unified fitting to reflect shape and surface morphology of the primary particles and the aggregates. As shown in Figure 5, the Porod exponent of the primary particles increases with increasing HAB and finally gets close to 4. According to the previous studies, P equal to 4 represents that the particles have smooth surfaces (Brumberger 2013), and the exponent between 3 and 4 implies rough surfaces. That is to say, in this study, the surfaces of the primary particles are flat and rough at low HABs and grow smoother with increasing HAB. In Figure 5, it is seen that $Ru(acac)_3$ addition decreases the P exponent of the primary soot particles, indicating that $Ru(acac)_3$ can depress the surface growth of the primary particles. It could be due to the inhibition effect of the metal additives on the growth of PAHs, which suppresses the process of PAH-soot surface addition. This is consistent with the report of Ritrievi, Longwell, and Sarofim (1987) who found the addition of ferrocene reduced the surface growth rate of soot particles. Similarly, in our previous study (Tang et al. 2019), it was found that nickel additive could delay the soot surface growth. Another possible explanation for the rough surfaces of the soot particles with $Ru(acac)_3$ addition is soot oxidation. Ru-based catalysts have high activity in the soot combustion and can promote soot oxidation significantly. As is proven in an earlier study (Over and Seitsonen 2002), the Ru–O bond is weak so that the dissociative adsorption of the active oxygen on the Ru site is easy to occur. Thus, the oxidation of organic species on the soot surface are facilitated in the $Ru(acac)_3$-doped flames, eventually leading to the formation of the primary soot particles with rough surfaces.

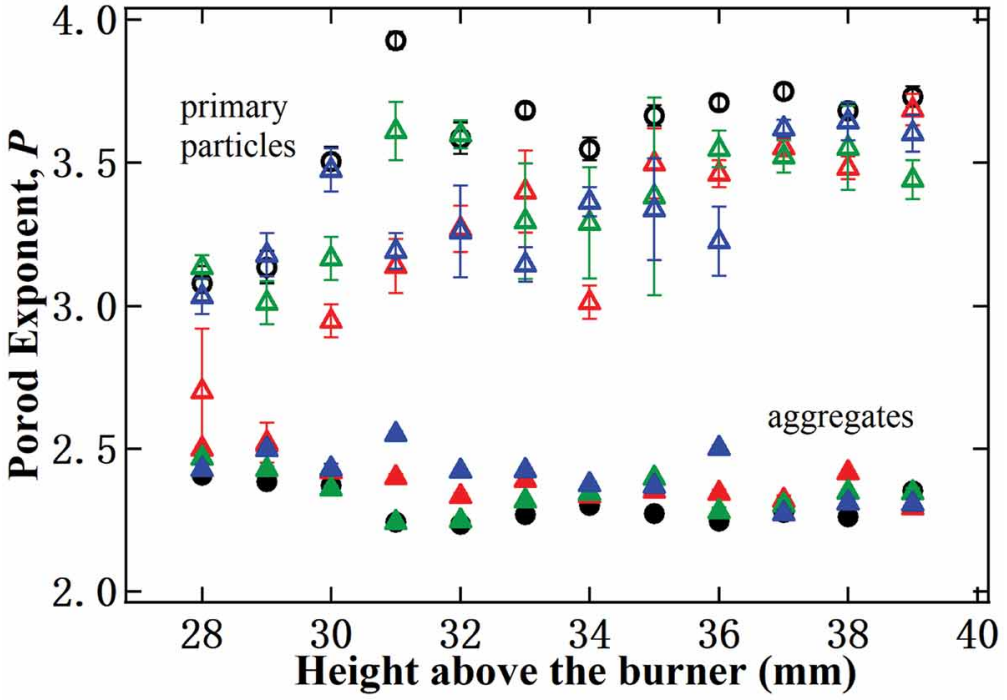

Figure 5. The Porod exponents of the primary particles (black open circles: undoped flame, red open triangles: 50 ppm $Ru(acac)_3$-doped flame, green open triangles: 100 ppm $Ru(acac)_3$-doped flame, blue open triangles: 150 ppm $Ru(acac)_3$-doped flame) and aggregates (black closed circles: undoped flame, red closed triangles: 50 ppm $Ru(acac)_3$-doped flame, green closed triangles: 100 ppm $Ru(acac)_3$-doped flame, blue closed triangles: 150 ppm $Ru(acac)_3$-doped flame)

In addition, the Porod exponent of the aggregates in both undoped and doped flames are between 2 and 2.5 as shown in Figure 5, and there is no significant difference found between different conditions. A exponent of three reflects a compact spherical particle, and a lower value indicates an aggregate with more fluffy and looser structure (Di Stasio et al. 2006). It means that in this work, the aggregates in all flames are formed loosely and behave as Gaussian polymer chains, which is in agreement with Figure 2. These results indicate that $Ru(acac)_3$ affects the morphology of the primary particles significantly, but slightly influence the aggregates.

Effect of catalysts on size and volume of soot particles

To investigate the effects of $Ru(acac)_3$ on the soot particle size, we obtain the radius of gyration, R_G of the primary particles by unified fitting. It has been elucidated that R_G can represent the real particle radius for poly-dispersed spheres (Beaucage, Kammler, Pratsinis 2004). The results of R_G are set out in Figure 6, showing that R_G grows as HAB increases, and then hits a plateau under all conditions. It means that the soot particles grow quickly in the low flame region and then tends to keep a steady size. In this figure, we can see that the additions of 50, 100 and 150 ppm catalysts all slightly abate R_G compared with the undoped flame. As we know, surface growth is an important process for soot particle size growing, and the particle size decreases during the oxidation process. Thus the primary soot particle size mainly relies on the net rate of surface reactions, i.e., competition between the oxidation and growth on the particle surface (Frenklach 2002). From Figure 5, we found that $Ru(acac)_3$ reduced the rate of the surface growth. Besides, it has been confirmed that the oxidative activity of the primary particles can be enhanced with the addition of Ru catalysts. Thus, the primary soot particles can be oxidized into much smaller ones after the addition of $Ru(acac)_3$, resulting in smaller soot particles in the doped fames compared with the undoped flame at the same HABs.

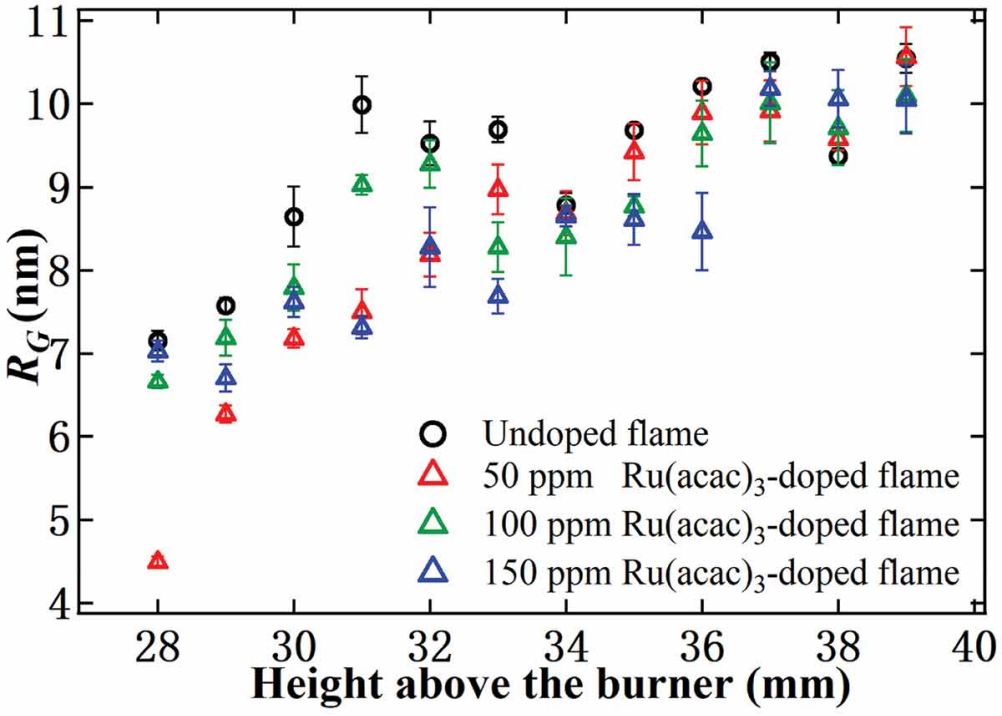

Figure 6. The radius of gyration with uncertainties for the primary particles as a function of HAB in the undoped flame, 50 ppm, 100 ppm and 150 ppm Ru(acac)$_3$-doped flame, respectively

The size distribution and the mean diameter of the primary soot particles in the undoped and doped flames were obtained by the TEM statistical analysis, and the results at different HABs are shown in Figure 7 and Figure 8, respectively. Compared with the primary soot particles in the undoped flame, the peak frequency of the diameter distribution shifts toward lower diameter in the doped flames. This change may come from the oxidation of the large particles. That is to say, the large particles are prone to be oxidized into smaller particles, which leads to the increase of the number proportion of the small particles and decrease of the number proportion of the larger particles, thus making the distribution curves concentrated around small diameter values. Besides, the average diameters of the primary particles also decrease in the doped flames, which is in accord with our observations for R_G from SAXS results in Figure 6.

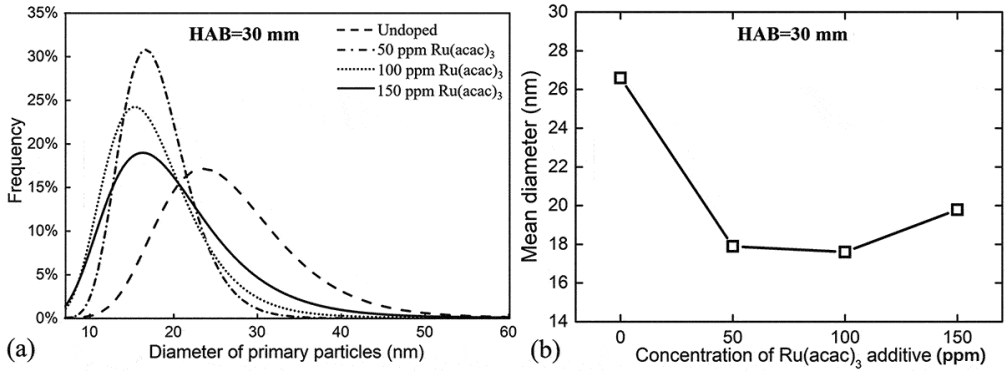

Figure 7. The primary particle size distributions and mean diameters of the soot particles in the undoped flame, 50 ppm, 100 ppm and 150 ppm Ru(acac)$_3$-doped flame at 30 mm HAB

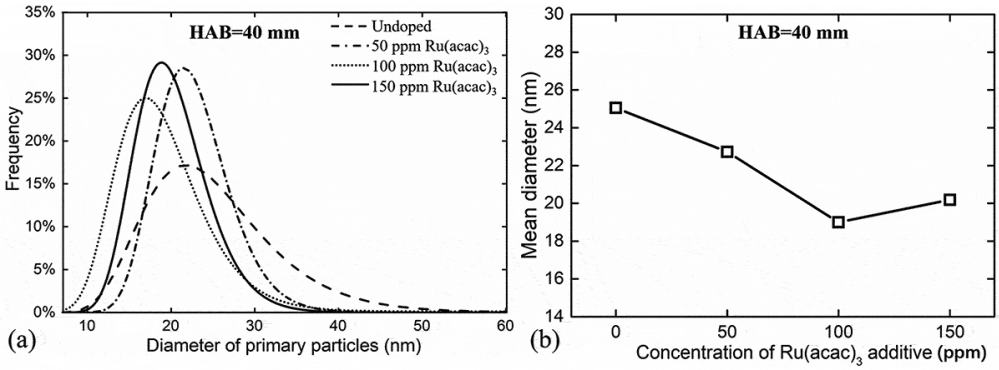

Figure 8. The particle size distributions and mean diameters of the primary soot particles in the undoped flame, 50 ppm, 100 ppm and 150 ppm $Ru(acac)_3$-doped flame at 40 mm HAB

According to the above discussion, $Ru(acac)_3$ catalysts affect the primary soot particles markedly in the process of the surface growth and oxidation. Figure 9 shows the proposed reaction mechanism of the soot combustion catalyzed by $Ru(acac)_3$. During the thermal decomposition of $Ru(acac)_3$ in the flames, Ru metal particles were generated initially and then they were oxidized into RuO_2 when the flame temperature reached a certain value according to the previous study (Musić et al. 2002). Villani et al. (2006), Tschamber et al. (2007) and Jeguirim et al. (2010) demonstrated that Ru surface was a generator of active oxygen species even at low temperatures. Chemisorption of oxygen on the sites of RuO_2 metal surfaces produces weakly bonded atomic oxygen with an extremely high chemical reactivity. The active oxygen radicals could migrate to the carbon surface, leading to a high concentration of surface oxygenated carbon complexes and making the carbon more susceptible to be oxidized. In addition, PAHs play a vital role in the soot surface growth. Metal catalysts can inhibit the surface growth rate of the soot particles and then make the soot surfaces rougher by decreasing the amount of PAHs. Based on these effects of $Ru(acac)_3$ on the process of surface growth and oxidation, the primary soot particles can grow into smaller particles with rougher surface in the doped flames.

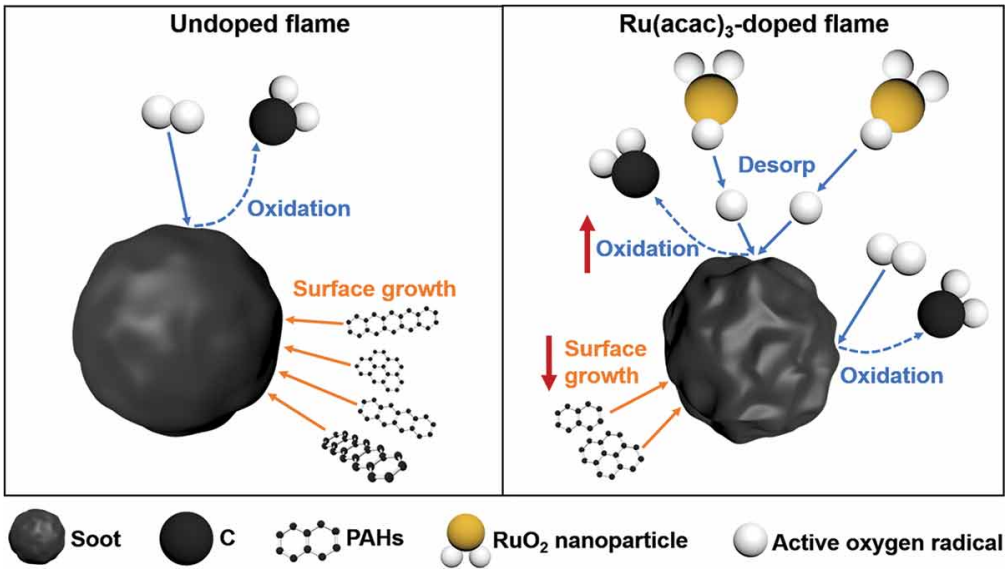

Figure 9. Predicted reaction mechanism of the soot combustion catalyzed by $Ru(acac)_3$.

The volume distribution of the soot particles at several selected HABs are obtained by using TNNLS fitting method and shown in Figure 10. It is suggested that the peak of the soot volume distribution shifts from 18 nm diameter to 22 nm diameter as HAB increases, indicating the particle size grows larger downstream along the flame centerline. Besides, the fluctuation shown at higher diameter and slight hoist

shown at lower diameter values are probably artifacts of the fitting procedure, and we can ignore these spikes. Another feature in these figures is that the volume distributions of the soot particles in the $Ru(acac)_3$-doped flames are much lower than those in the undoped flame at almost each same HAB. However, there is not a clear trend between different concentration of the catalysts.

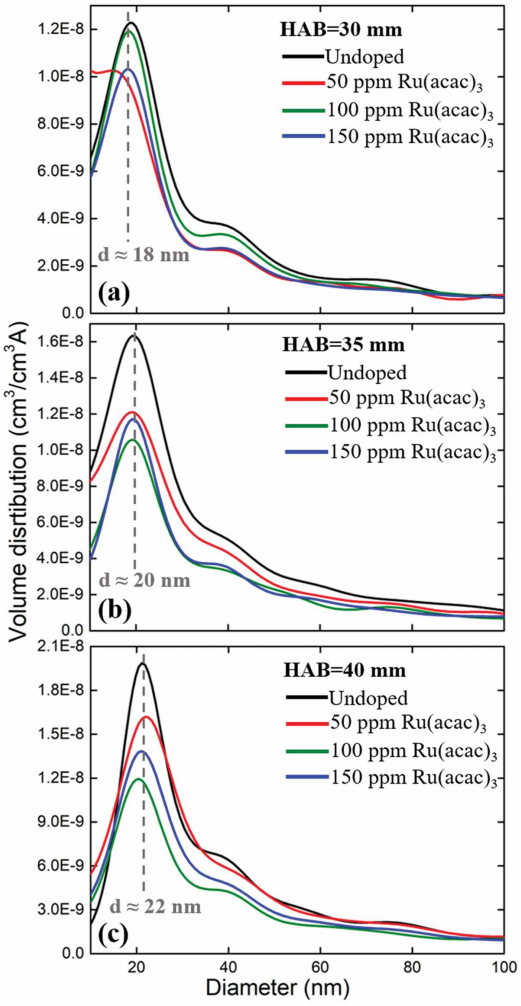

Figure 10. The volume distributions of the soot particles by TNNLS at 30, 35 and 40 mm HABs in the undoped flame, 50 ppm, 100 ppm, and 150 ppm $Ru(acac)_3$-doped flame, respectively

Shown in Figure 11 are the volume fractions of the soot particles obtained by Eq. (8) and Eq. (9) by assuming the particles are homogeneous. Thus, the uncertainties of scattered intensity will pass to the calculated volume fractions of the soot particles, and the uncertainties of the volume fractions are also presented in the figure. As can be seen, the volume fraction increases with increasing HAB in both undoped and doped flames. The volume fraction is, respectively, reduced after the addition of 50, 100, or 150 ppm $Ru(acac)_3$, which means that $Ru(acac)_3$ suppresses the soot volume. The previous studies found that Ru is an effective catalyst or catalyst promoter for soot oxidation (Castoldi et al. 2017; Villani et al. 2006). In our work, the Porod exponent of the primary particles apparently decrease after adding $Ru(acac)_3$ catalyst, meaning a suppression effect in the surface growth rate of the primary soot particles. Therefore, the size of the primary particles decreases due to the effects of rapid oxidation and slow surface growth. All of these effects could be the reasons to lead to a descent in the volume fraction. However, it should be noted that the scattering length density of carbon was used as the contrast scattering length in the data analysis, so the actual contrast length density should be a little smaller than that of carbon, and for each soot particle, the contrast scattering length could be different. Therefore, the actual volume fractions of the soot should be slightly smaller than the results shown in Figure 11.

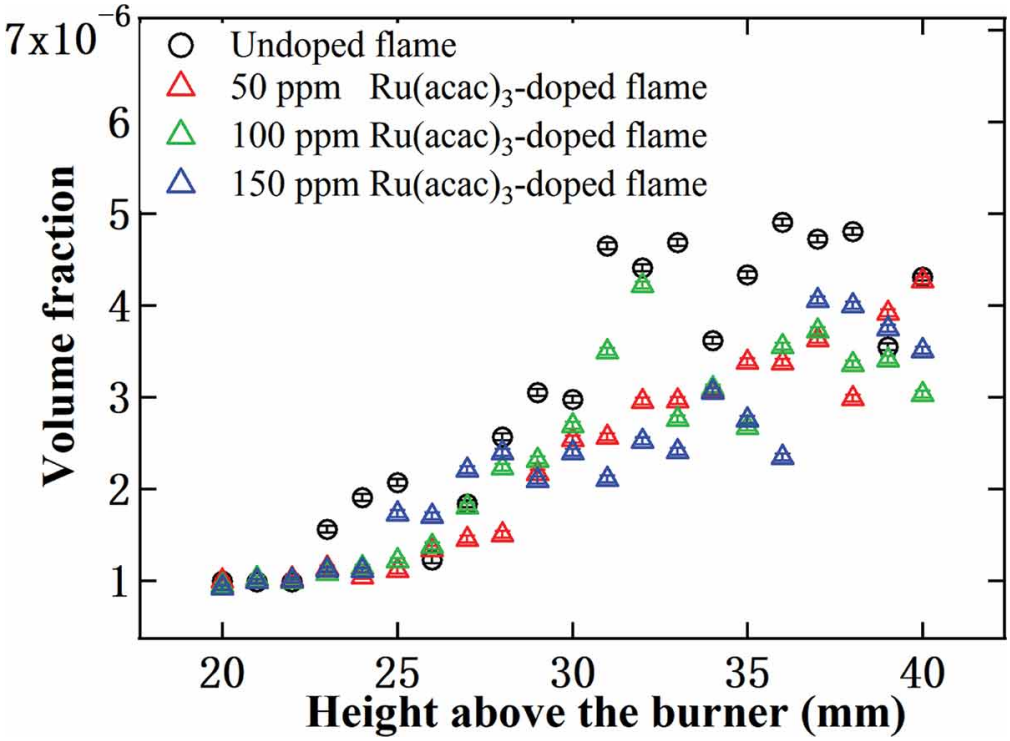

Figure 11. The volume fractions and their uncertainties of the soot particles generated in the undoped flame, 50 ppm, 100 ppm, and 150 ppm $Ru(acac)_3$-doped flame, respectively

Together, these results provide some evidence on how the $Ru(acac)_3$ catalysts affect the soot particles. Prior study (Frenklach 2002) noted that the soot mass accumulated is determined primarily by surface reactions, i.e., growth and oxidation. While the surface growth can lead to an increase in the particle size and the soot volume fraction, soot oxidation plays the opposite role. In this study, Ru and RuO_2 nanoparticles produced by the thermal decomposition of $Ru(acac)_3$ promote the oxidation reactions between oxygen and soot. Molecular oxygen O_2 can be easily adsorbed on the surface of metal nanoparticles and turn into various active forms, and thus participate in the soot oxidation reactions. Besides, $Ru(acac)_3$ can reduce the amount of the surface growth precursors, e.g., PAHs. And then inhibit the surface growth for the primary soot particles. Overall, these results indicate that the primary soot particles grow into smaller particles with rougher surfaces in the doped flames than those in the undoped flame due to the combined effects of the surface growth and oxidation. However, no clear trend is observed in the soot particle size and volume among the three flame groups doped with 50, 100, or 150 ppm $Ru(acac)_3$. A further study on whether more intensive concentration intervals can make a difference will be performed.

In addition, we should mention that this work only provides a fundamental investigation on soot emission under catalytic combustion. Application of this method on soot reduction in real combustors will require further studies and simulations possibly involving design of specific catalytic chamber. Moreover, the metal particles should not be released into the atmosphere maybe by some treatment in the exhaust pipe, which will be a different subject needed for further investigations.

4. Conclusions

The present study investigated the impacts of $Ru(acac)_3$ catalyst on the soot particles in the growth and oxidation process. *In-situ* SAXS experiment was performed to get the information of the morphology, size and volume fraction of the soot particles. Besides, TEM was used to support our results by direct observation of the soot morphology and statistical analysis.

Based on the foregoing results and discussion, it was found that the catalysts can suppress the surface growth for the primary soot particles, leading to rougher surfaces, while they rarely affect the aggregates. Thus, the primary particle size significantly decreases due to the slow surface growth and the rapid oxidation effects in the doped flames. The maximum frequency of the diameter distribution shifts to a lower

diameter after the addition of $Ru(acac)_3$. Compared with the undoped flame, the volume fraction of the soot particles is reduced in the $Ru(acac)_3$-doped flames. As a result, $Ru(acac)_3$ inhibits soot emission effectively. However, no clear trend can be obtained from the concentration change of $Ru(acac)_3$. Wider concentration range of the catalyst may provide more information. Further research will be conducted to explore the effect from the composition change of the catalyst and detect the intermediate species produced in the combustion process to establish a detailed mechanism.

Acknowledgment

The authors gratefully acknowledge the National Natural Science Foundation of China (the grant number U2032119, 91641125 and 71690245) for their financial support. We also thank for the “IRENA” micro package provided by Dr. Jan Ilavsky for data fitting. Besides, we would like to acknowledge Yuchen Zhu, a PhD student in University of Science and Technology Beijing, for his advice in TEM analysis. This research was performed at the APS, a U.S. Department of Energy (DOE) Office of Science User Facility under Contract No. DE-AC02-06CH11357.

Disclosure statement

The authors declare that they have no known competing financial interests or personal relationships that could have appeared to influence the work reported in this paper.

Funding

This work was supported by the National Natural Science Foundation of China [71690245,91641125,U2032119].